DOI: https://doi.org/10.67656/njmse.2024.nq10umfh

Onuoha *et al.*: Nigerian Journal of Materials Science and Engineering. Vol. 14 (1): 1 - 7 (2024)

Influence of Weight Fraction on the Average Crystallite Size of Hybrid ZnO/Al_2O_3 Supported Bio-Waste Activated Carbon Composites

[1*]Onuoha David Chikaorama, Egbe Evudiovo Apha Peter, [2]Abdulrahman Asipita Salawu and [3]Abdulkareem Ambali Saka

[1*]Mechanical Engineering Department, Federal University of Technology, P.M.B 65 Minna, Niger State. Nigeria.
[2]Materials and Metallurgical Engineering Department, Federal University of Technology, P.M.B 65 Minna, Niger State. Nigeria.
[3]Chemical Engineering Department, Federal University of Technology, P.M.B 65 Minna, Niger State. Nigeria.
*Corresponding author: chika.onuoha@cstd.nasrda.gov.ng

Abstract

Due to the inherent high surface energy and the multifaceted interaction between them and the matrix interface, metal nanoparticles tend to coalesce in the absence of repulsive forces provided by a capping agent. It is therefore imperative to provide a support system that will moderate the spatial behaviour of the particles to prevent the formation of bulk particles and eventually deteriorate in quality. This paper reports the influence of weight fraction on the average crystallite size of Al_2O_3 introduced onto formulated ZnO groundnut shell activated carbon (GSAC) supported composites. Al_2O_3 was synthesised using the sol-gel technique with aluminium trichloride as precursor salt. The surface morphology and average particle size of synthesised Al_2O_3 were determined using scanning electron microscopy (SEM) and transmission electron microscope (TEM), respectively. Al_2O_3 was introduced onto formulated GSAC/ZnO mixture at varying weight percentages (75:25, 50:50 and 25:75) to produce GSAC-ZnO/Al_2O_3 composites. The resulting composites were then characterised using X-ray diffraction (XRD). Relying on lattice parameters such as diffraction peaks and full width at half maximum (FWHM) obtained from the X-ray powder diffraction, the effects of weight fraction on the average crystallite size of ZnO/Al_2O_3 supported GSAC composites were determined using the Scherrer equation. The result obtained showed an increase in average crystallite size with the increase in amount of Al_2O_3 introduced onto the formulated GSAC/ZnO composite, but declined with further addition of Al_2O_3. The GSAC-ZnO/Al_2O_3 composite with a 75:25 weight fraction was found to have the smallest average crystallite size of 52.25 nm. The results suggest that the stabilisation influence of GSAC on ZnO and Al_2O_3 is reduced with an increase in the amount of Al_2O_3 and the tendency for agglomeration of ZnO and Al_2O_3 ions may have been weakened with the addition of more Al_2O_3, resulting in a decrease in crystallite size.

Keywords: Groundnut Shell, Activated Carbon, X-Ray Diffraction, Crystallite Size, Debye-Scherrer Method

1.0. INTRODUCTION

Carbonaceous materials with large internal surface area and well-developed porosity are being used as solid support for stabilising highly randomised metal nanoparticles (Maraise *et al*., 2013, Nouaamane *et al*., 2022). The support system serves to prevent metal nanoparticles ions from coalescing into bulk particles, which may lead to a decline in mechanical and corrosion resistance properties of composites (Roya and Trung, 2022). (Alojz and Ema, 2022) submitted that practically any type of metal oxide can be deposited on the cellulose surface with TiO_2, Fe_3O_4 and ZnO being the most abundant. Hamid and Seyyed (2014) studied the effect in terms of mechanical properties of 21 nm titanium dioxide nanoparticles in a vinyl ester resin and suggested that incorporation of particles into the polymer can result in a considerable improvement of mechanical properties, but however stated that a homogeneneous distribution of fillers within the matrix is essential in achieving the desired result. Sun *et al* (2008); Ramezanzadeha *et al* (2011) have submitted that nanoparticles could enhance their interaction with the matrix through chemical bonds. They could increase the cross-linking densities in the coatings or increase the physical interactions between macro-molecular chains of the matrix. Shi *et al* (2009) have said that matrix support for nanoparticles could be an effective means for nanoparticles to complement the poor mechanical and tribological performances of some polymer matrices, such as their poor resistance to surface abrasion and wear.

A good design of metal nanoparticles supported matrix composites could modify the composite system into desirable physical characteristics by taking into account the complex interaction between the matrix interface and nanoparticles (Hanemenn and Szabo, 2010). Essentially, when adsorbate ions are adsorbed on the surface of an adsorbent, there is a restriction of movement of adsorbate ions, resulting in a decrease in the degree of randomness of the system and eventual decrease in entropy. Grain boundaries are initiated and the inability of the ions to cross the grain boundaries enhances the system's micro-hardness property and its corrosion resistance ability due to finer surface finishing.

Dispersion hardness, self-lubricity, high temperature inertness, good wear and corrosion resistance, as well as chemical and biological compatibility are all common properties of ceramic or metal matrix nanocomposites with an extra dispersed phase of particulates (Shei *et al*., 2005).

Onuoha *et al*., 2020 have reported that generally desired material properties such as improved toughness, increased hardness and enhanced corrosion resistance of nano-structured systems are strongly crystallite size and grain size dependent. Smaller crystallite sizes result in a drastic reduction in the required diffusing path for ions, thereby enhancing system sorption kinetics significantly (Gubicza, 2017). It is therefore imperative to evaluate the effects of weight fraction on the average crystallite size of Al_2O_3 introduced onto prepared ZnO supported groundnut shell activated carbon composites using one of the widely used tools (Scherrer equation), which has been well explained in our previous work (Onuoha *et al*., 2020). The results obtained may be vital for the engineering applications of the resulting composites.

2.0 MATERIALS AND METHODS

2.1 Materials

Some of the chemical reagents and equipment used are as reported by (Onuoha *et al*., 2020). The chemicals and reagents used in the synthesis of Al_2O_3 include ammonia, ethanolic and 0.1M aluminum trichloride ($AlCl_3$)

2.2 Methodology

2.2.1 Preparation of groundnut shell activated carbon (GSAC) and ZnO

The bio-waste activated carbon used in this work was sourced from groundnut shell and ZnO synthesised from 100 ml of isopropyl alcohol and 15 ml of zinc acetate dehydrate (Zn (CH_3COO) $2H_2O$), following the procedures well described in our previous work (Onuoha *et al*., 2020).

2.2.2 Synthesis of Al_2O_3

To synthesise Al_2O_3 using the sol-gel method, aluminium trichloride was used as the precursor. 28% of ammonia was introduced dropwise to a stirred ethanolic solution of aluminium chloride (0.1M). The formed gel was left to mature for 30 h at room temperature after filtering in a vacuum chamber, drying at 100 ºC for 24 h in an oven and annealed at 1000 ºC. The formation and morphology of Al_2O_3 were confirmed by TEM and SEM analysis, respectively.

2.2.4 Formulation of GSAC-ZnO/Al_2O_3 Composites

Al_2O_3 was introduced onto GSAC/ZnO sample mixture (A:75 wt.% of GSAC and 25 wt % of ZnO) which presented the smallest average crystallite size as reported by (Onuoha *et al*., 2020). Three (3) composites (A^1, B^2 and C^1) with varying weight percentage compositions of GSAC/ZnO doped with Al_2O_3 at (A^1:75 wt.% of GSAC/ZnO and 25 wt. % of Al_2O_3); (B^1:50 wt.% of GSAC/ZnO and 50 wt.% of Al_2O_3) and (C^1:25 wt.% of GSAC/ZnO and 75 wt.% of Al_2O_3 were formulated. To prepare the composites, each set of combination mixture was dissolved in 50 ml of acetone and stirred vigorously using a magnetic stirrer at 30 rpm for 25 min to achieve homogeneity and even distribution of the constituents. The slurry formed was heated in an oven at 60°C for 4 h to eliminate acetone (Lusi *et al*., 2017). XRD analysis of the different mixture ratios was carried out and their average crystallite sizes (D) were calculated using the Debye-Scherrer equation given by (Onuoha *et al*., 2020)

3.0 RESULTS AND DISCUSSION

3.1 Characterisation of GSAC and ZnO

The results of the proximate, FTIR and SEM analysis for GSAC, as well as the TEM, SEM and XRD analysis for ZnO have been presented by (Onuoha *et al*., 2020).

3.2 Characterisation of Al_2O_3

The Scanning Electron Microscopy coupled with Energy Dispersive Spectroscopy (SEM-EDS) analysis of the synthesised aluminium oxide (Al_2O_3) nanoparticles was conducted and the results are depicted in Figure 1. The SEM micrographs revealed that the Al_2O_3 particles exhibited predominantly spherical morphology with smooth surfaces and uniformly distributed nanograin structures. The fine particle size and regular shape suggest effective control over the synthesis parameters, which is critical for applications that require high surface area and structural homogeneity (Yoldas, 1975; Zhang *et al.,* 2018).

Notably, the SEM images showed no visible surface defects such as irregular patches or particulate clusters that could be indicative of contamination. The absence of extraneous dots or coloured regions further implies a high degree of purity in the prepared sample. This morphological consistency is a desirable feature in nanoparticulate materials, as it enhances reproducibility in both structural and functional performance (Lu *et al.,* 2007).

The Energy Dispersive Spectroscopy (EDS) spectrum further confirmed the elemental composition of the sample. A prominent peak corresponding to aluminium (Al) was observed at approximately 1.48 keV, which is characteristic of Al Kα emission. This spectral signature validates the presence of aluminium in the oxide form and the absence of additional peaks suggests that no foreign elements or impurities were introduced during the synthesis process (Goldstein *et al.,* 2018). EDS,

while semi-quantitative, is an effective tool for rapid elemental verification and its application here reinforces the integrity of the synthesis procedure used for Al_2O_3 production.

Together, the SEM-EDS results confirm the successful fabrication of high-purity, nanoscale Al_2O_3 with favourable morphological features, rendering it suitable for use in various high-performance applications such as ceramics, catalysis and electronic substrates.

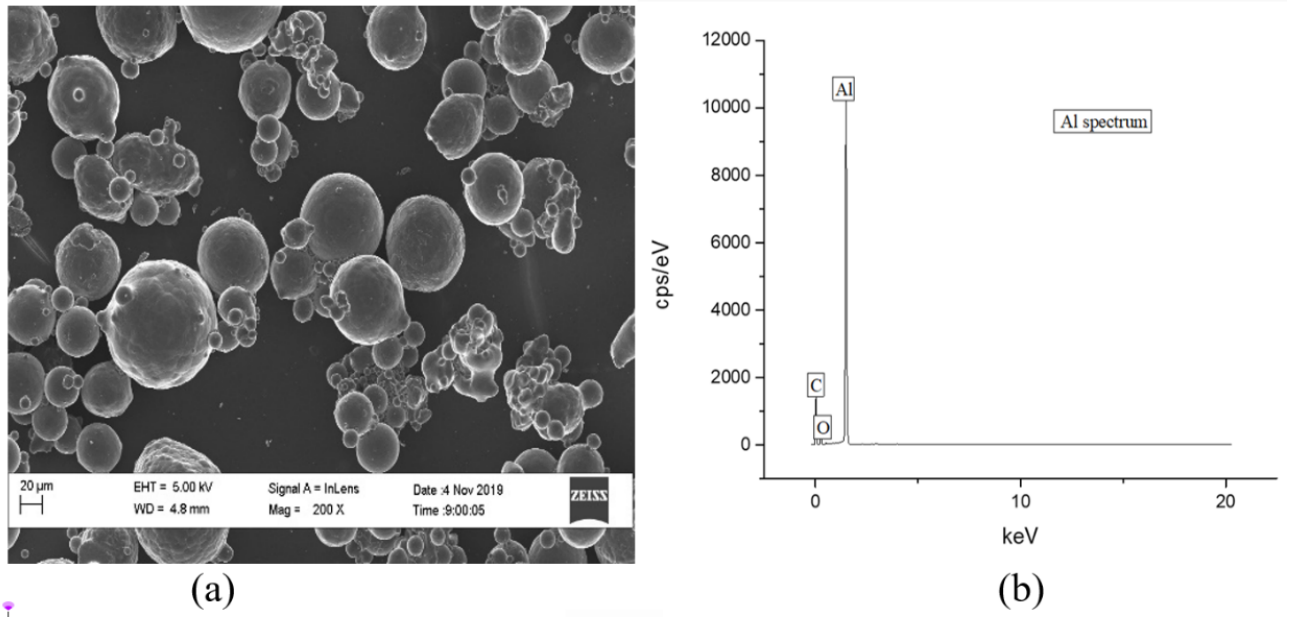

Figure 1: (a) SEM micrograph for Al_2O_3 and (b) EDS spectrum

The Transmission Electron Microscopy (TEM) micrographs of the synthesised aluminium oxide (Al_2O_3) nanoparticles, as illustrated in Figure 2, reveal a predominantly fine-grained and homogeneously dispersed internal structure. This microstructural uniformity is indicative of successful synthesis and a controlled nucleation process during preparation. Nevertheless, isolated zones of agglomeration are evident within the micrographs. These agglomerations are most likely attributed to the inherently high surface energy and large surface-to-volume ratio characteristic of metal and metal oxide nanoparticles, which render them thermodynamically unstable in dispersed forms (Gleiter, 2000).

Such agglomeration is a common phenomenon in nanoparticle systems and is often driven by van der Waals forces and magnetic or electrostatic interactions, which facilitate particle–particle contact and clustering (Park *et al.,* 2007). In the absence of sufficient surface modification or stabilising agents, the nanoparticles tend to coalesce in order to reduce their overall surface energy and achieve a lower-energy state. This behaviour is particularly pronounced in oxide systems such as Al_2O_3, where the particles may lack adequate surface functionalisation to repel one another in suspension or dry form (Zhang & Banfield, 2000).

While mild agglomeration does not necessarily compromise the structural integrity or functionality of the material, it can affect specific surface area, porosity and performance in applications such as catalysis, adsorption, or as a ceramic reinforcement phase. To mitigate such agglomeration, surface treatments using organic ligands, surfactants, or mechanical dispersion techniques (e.g., ultrasonication) are often employed during synthesis or post-processing (Mourdikoudis *et al.,* 2018).

However, the TEM images confirm the synthesis of fine, nanoscale Al_2O_3 particles with generally good dispersion.

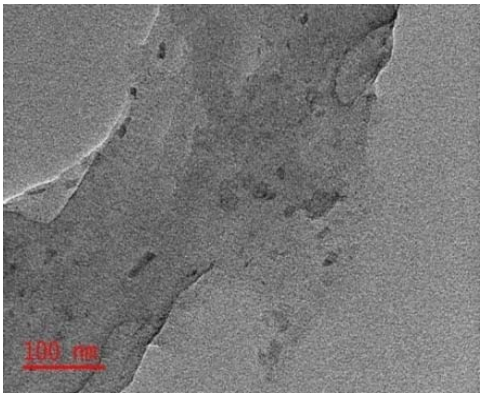

Figure 2: TEM micrograph for Al_2O_3

The XRD patterns shown in Figure 3 for the GSAC-Zn/Al_2O_3 mixture at different ratios (75 wt.% of GSAC-ZnO and 25 wt % of Al_2O_3), (50 wt.% of GSAC-ZnO and 50 wt.% of Al_2O_3) and (25 wt.% of GSAC-ZnO and 75 wt.% of Al_2O_3) revealed sharp diffraction peaks for the three mixture ratios, which suggested well-crystallised samples. This is in agreement with Irfan *et al* (2018), which stated that strong, sharp and narrow diffraction peaks show that the synthesised product was well crystallised.

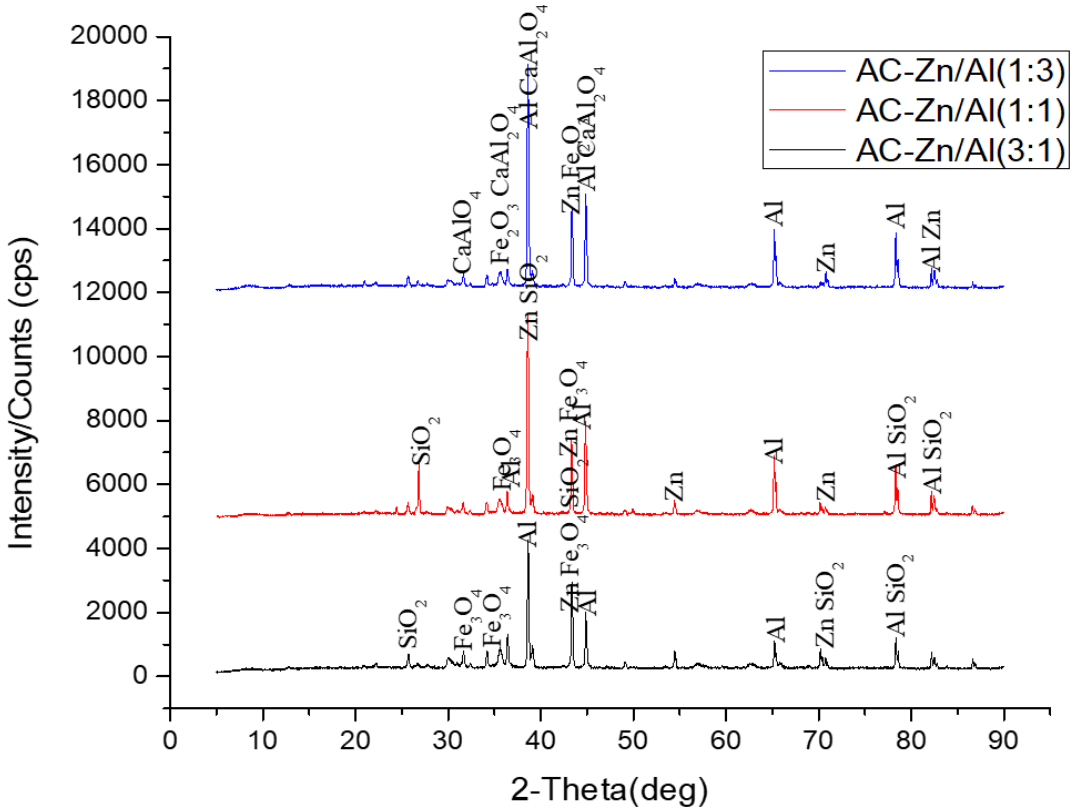

Figure 3: XRD patterns for GSAC-ZnO/Al_2O_3 composites

3.4 Determination of Average Crystal Size

Table 1 presents the calculated average crystallite sizes of the synthesized GSAC-ZnO/Al_2O_3 composite materials with varying weight ratios: A1 (75 wt.% GSAC-ZnO and 25 wt.% Al_2O_3), B1 (50 wt.% GSAC-ZnO and 50 wt.% Al_2O_3) and C1 (25 wt.% GSAC-ZnO and 75 wt.% Al_2O_3). The crystallite size analysis, based on X-ray diffraction (XRD) data and calculated using the Debye–Scherrer equation, reveals a non-linear trend in particle growth with respect to increasing Al_2O_3 content. Specifically, the crystallite size increased from 52.25 nm in composite A1 to a maximum of 58.72 nm in composite B1, followed by a decrease to 54.00 nm in composite C1. This trend indicates that the optimal crystallite growth occurs at an equimolar mixture of GSAC-ZnO and Al_2O_3.

The observed variation in crystallite size can be attributed to the influence of Al_2O_3 on the microstructural evolution of the composites. At lower Al_2O_3 concentrations (composite A1), ZnO predominates, potentially promoting the nucleation of smaller crystallites. As the Al_2O_3 content increases to 50 wt.% (composite B1), there is a balanced interaction between Al_2O_3 and ZnO species, possibly enhancing interfacial diffusion and crystallite growth due to synergistic effects (Wang *et al.,* 2016). However, with further addition of Al_2O_3 to 75 wt.% in composite C1, the crystallite size declines, likely due to the dilution of ZnO active sites and reduced inter-metallic interactions. The excess of Al_2O_3 ions may dominate the matrix, disrupting the thermodynamically favored pathway toward bulk crystallite formation and hindering effective grain growth (Tadic *et al.,* 2014).

The observed crystallite size sequence (A1 < C1 < B1) suggests that an intermediate ratio of ZnO and Al_2O_3 promotes the most efficient crystallite development. This phenomenon aligns with earlier findings that highlight the importance of compositional balance in nanocomposite systems for optimizing microstructural and functional properties (Zhang *et al.,* 2018).

Table 1: Calculated Average Crystallite Size and Micro Strain of GSAC-ZnO/Al_2O_3 Different Mixture Ratios

Sample ratio	Pos (2θ)	Height (cts)	FWHM (β)	d-spacing (Å)	Rel. Int (%)	Crystallite size (G) (nm)
AC-ZnO/ Al_2O_3 3:1	25.719	399.995	0.315	3.464	10.470	27.04
	30.125	228.947	0.630	2.967	6.000	13.65
	35.579	513.701	0.394	2.523	13.450	22.13
	36.493	963.437	0.157	2.466	25.230	55.69
	38.591	3818.649	0.118	2.333	100.000	74.56
	39.134	644.032	0.197	2.302	16.870	44.73
	43.338	2571.927	0.118	2.088	67.350	75.72
	44.833	1646.232	0.118	2.022	43.110	76.12
	65.239	832.876	0.118	1.430	21.810	83.55
	70.482	230.997	0.944	1.336	6.050	10.77
	78.347	948.433	0.118	1.220	24.840	90.77
Average crystalline size (nm)						**52.25**
AC-ZnO/ Al_2O_3 1:1	26.836	1604.326	0.118	3.322	27.820	72.35
	35.527	386.221	0.394	2.527	6.700	22.13
	38.645	5767.809	0.148	2.330	100.000	59.46
	43.311	2303.732	0.098	2.089	39.940	91.17
	44.782	2322.220	0.157	2.024	40.260	57.20
	54.428	388.449	0.236	1.686	6.730	39.56
	65.193	1825.821	0.098	1.431	31.660	100.57
	70.258	211.434	0.787	1.340	3.670	12.13
	78.312	1538.786	0.098	1.221	26.680	109.27
	82.369	370.072	0.472	1.171	6.420	23.38
Average crystalline size (nm)						**58.72**
AC-ZnO/ Al_2O_3 1:3		155.694	0.630	2.966	2.370	13.65
		394.889	0.394	2.523	6.010	22.13
		6575.789	0.098	2.334	100.000	89.77
		2339.327	0.118	2.088	35.570	75.72
		2661.635	0.117	2.022	40.480	76.77
		1727.888	0.118	1.431	26.280	83.53
		310.327	0.630	1.330	4.720	16.17
		1664.475	0.118	1.221	25.310	90.76
		338.733	0.630	1.170	5.150	17.52
Average crystalline size (nm)						**54.00**

4.0 CONCLUSION

Al_2O_3 which was synthesized using the Sol-gel method, was successfully introduced onto groundnut shell activated carbon/ZnO (GSAC/ZnO) composite formulated by (Onuoha *et al*., 2020) at three varying weight fractions (A^1:75 wt.% of GSAC/ZnO and 25 wt. % of Al_2O_3); (B^1:50 wt.% of GSAC/ZnO and 50 wt.% of Al_2O_3) and (C^1:25 wt.% of GSAC/ZnO and 75 wt.% of Al_2O_3 to give three different composites, A^1, B^2 and C^1. The average crystallites sizes of the composites determined using Debye-Scherrer equation, demonstrated a good interaction among the participating samples with GSAC retaining its efficient stabilization property for the hybrid metal oxides. However, it was noted that the composite with the least weight percentage of Al_2O_3 gave the smallest average crystallite size of 52.25 nm, suggesting that with smaller amount of Al_2O_3 present in the composites, GSAC tended to effectively moderate the spatial behaviour of ZnO and Al_2O_3 by preventing ZnO Al_2O_3 ions from coalescing to each other to give bulk particles, thereby deteriorating in quality. However, it was noted that the average crystallite size declined with further increase in the amount of Al_2O_3 introduce onto the prepared ZnO supported GSAC composite. This could be because further increase in the amount of Al_2O_3 in the system may have served to weaken the tendency for ZnO and Al_2O_3 to agglomerate, resulting in decrease in crystallite size

References

Alojz Anžlovar and Ema Žagar Cellulose Structures as a Support or Template for Inorganic Nanostructures and Their Assemblies Nanomaterials 2022, 12(11), 1837

Gleiter, H. (2000). Nanostructured materials: Basic concepts and microstructure. *Acta Materialia*, 48(1), 1–29. https://doi.org/10.1016/S1359-6454(99)00285-2

Goldstein, J. I., Newbury, D. E., Michael, J. R., Ritchie, N. W. M., Scott, J. H. J., & Joy, D. C. (2018). *Scanning electron microscopy and X-ray microanalysis* (4th ed.). Springer. https://doi.org/10.1007/978-1-4939-6676-9

Gubi c z a J. (2017). Re l a tionship be twe en Microstructure and Hydrogen Storage Properties of Nanomaterials. Defect Structure and Properties of Nanomaterials 2 and Extended Edition, 297 – 315

Hamid, S. and Seyyed, A. J. J. (2014) Effects of Titanium Dioxide Nanoparticles on the Mechanicle Properties of Vinyl Ester-Based Nanocomposites. *J Comp Mat* 2014 vol 49 iss 19 pp 2365-2373

Hanemann T and Szabo, D. V. (2010) Polymer - Nanoparticle Composites: From Synthesis to Modern Applications. Materials 2010 3(6) 3468 – 3517

Irfan, H., Mohamed, R. K. and Anand, S. (2018) Microstructural Evaluation of $CoAl_2O_4$ Nanoparticles by Williamson-Hall and Size-Strain Plot Method. *Journal of Asian Ceramic Societies* vol. 6, (2018) issue 1.

Lu, L., Shen, Y., Chen, X., & Qian, X. (2007). Synthesis of alumina nanoparticles with tunable morphology and crystal phase. *Journal of Crystal Growth*, 304(2), 369–374. https://doi.org/10.1016/j.jcrysgro.2007.03.029

Lusi, E., Ratna, B., Takashi, O., Kikuo, O. and Tomonori, T. (2017) Role of Acetone in the Formation of Highly Dispersed Cationic Polystyrene Nanoparticles. *Chemical and Process Engineering*, 2017, 38(1), 5 – 18

Maraísa G., Mário C. G., Luiz Carlos, A. O. and Cinthia, S. C. A (2013). Friendly Environmental Material: Iron Oxide Dispersed over Activated Carbon from Coffee Husk for Organic Pollutants Removal. *Journal of Environmental Management* Volume 127, 30 September 2013, Pages 206-211

Mervat, F. Z., Wael, H. E.and Badawi, A. (2022). Garlic Peel as Promising Low-cost Support for the Cobalt Nanocatalyst: Synthesis and Catalytic Studies. *Journal of Environmental Management* Volume 312, 15 June 2022, 114919

Mourdikoudis, S., Pallares, R. M., & Thanh, N. T. K. (2018). Characterisation techniques for nanoparticles: Comparison and complementarity upon studying nanoparticle properties. *Nanoscale*, 10(27), 12871–12934. https://doi.org/10.1039/C8NR02278J

Nouaamane, I., Larbi, B., Nicolas, M., Philippe, Z. and Hamid, K. (2022). Comprehensive Preparation and Catalytic Activities of Co/TEMPO-Cellulose Nanocomposites: A Promising Green Catalyst Carbohydrate. *Polymers* Volume 295, 1 November 2022, 119765

Onuoha, D. C., Egbe, E. A. P., Abdulrahman, A. S. and Abdulkareem, A. S. (2020). Evaluation of the Effects of Weight Fractions on the Average Crystallite Size of ZnO Supported Bio-Waste Activated Carbon Composites. *Nigerian Journal of Materials Science and Engineering*. Vol. 10(2):60 - 67 (2020)

Park, J., An, K., Hwang, Y., Park, J. G., Noh, H. J., Kim, J. Y., … Hyeon, T. (2007). Ultra-large-scale syntheses of monodisperse nanocrystals. *Nature Materials*, 3(12), 891–895. https://doi.org/10.1038/nmat1251

Ramezanzadeha, B., Attara, M. M. and Farzamb, M. (2011) A Study on the Anticorrosion Performance of the Epoxy-polyamide Nanocomposites Containing ZnO Nanoparticles Pro. Org. Coating 2011 72 410 - 22

Roya, T. and Trung, D. (2022). Noble Metal Nanoparticles Dispersed on Nanocellulose: Agreen Platform for Catalytic Organic Transformations 2022 Conf. Ser.: Mater. Sci. Eng. 1258 012014 DOI 10.1088/1757-899X/1258/1/012014

Shei, L., Sun, C., Gao, P., Zhou, F. & Liu, W. (2005) Mechanical Properties and Water and Corrosion Resisitance of Electrodeposited Ni-Co/SiC Nanocomposite Coating. Applied Surface Science 252(2006) 3591-3599

Shi, X. M., Nguyen, T. A., Suo, Z. and Liu, Y. (2009) Effect of Nanoparticles on the Anticorrosion and Mechanical Properties of Epoxy Coating Surf. Coat. Technol. 204 (3) 237–45 2009.

Tadic, M., Panjan, M., Damnjanovic, V., Milosevic, I., & Jokanovic, V. (2014). Structural and magnetic properties of ZnO:Fe nanoparticles prepared by sol–gel method. *Materials Chemistry and Physics*, 147(1–2), 33–40. https://doi.org/10.1016/j.matchemphys.2014.04.045

Wang, Z., Wang, Z., Sun, J., & Li, X. (2016). Synthesis and characterization of ZnO–Al_2O_3 nanocomposites with enhanced photocatalytic activity. *Ceramics International*, 42(6), 7527–

7533. https://doi.org/10.1016/j.ceramint.2016.01.120

Yoldas, B. E. (1975). Investigations of porous oxide glasses formed by hydrolysis of aluminium alkoxides. *Journal of Materials Science*, 10(11), 1856–1860. https://doi.org/10.1007/BF00554945

Zhang, Y., Chen, Y., Liu, H., & Zhang, H. (2018). Effect of Al_2O_3 content on the microstructure and properties of ZnO–Al_2O_3 composite ceramics. *Journal of Alloys and Compounds*, 764, 679–685. https://doi.org/10.1016/j.jallcom.2018.06.057

Zhang, H., & Banfield, J. F. (2000). Understanding polymorphic phase transformation behaviour during growth of nanocrystalline aggregates: Insights from TiO_2. *Journal of Physical Chemistry B*, 104(15), 3481–3487. https://doi.org/10.1021/jp993819z

Zhang, Y., Chen, Y., Liu, H., & Zhang, H. (2018). Effect of Al_2O_3 content on the microstructure and properties of ZnO–Al_2O_3 composite ceramics. *Journal of Alloys and Compounds*, 764, 679–685. https://doi.org/10.1016/j.jallcom.2018.06.057